Supplement of Earth Surf. Dynam., 10, 209–227, 2022
https://doi.org/10.5194/esurf-10-209-2022-supplement

Earth Surface Dynamics
Open Access
EGU

Supplement of

Comparative analysis of the Copernicus, TanDEM-X, and UAV-SfM digital elevation models to estimate lavaka (gully) volumes and mobilization rates in the Lake Alaotra region (Madagascar)

Liesa Brosens et al.

Correspondence to: Liesa Brosens (liesa.brosens@kuleuven.be)

Text S1 MoransI

We have verified the assumption of perfect autorcorrelation for the HEM pixels of a lavaka by calculating Moran's I (queen). For the TanDEM-X DEM the HEM-pixels of a lavaka have a mean Moran's I of 0.65 with a median of 0.70. For the Copernicus DEM these values are lower and equal to 0.31 and 0.38 for the mean and median, respectively (Fig. S4(b)). These results indicate that using the same HEM value for a full lavaka will result in a maximum estimate of the uncertainty, as in reality the pixels are not perfectly autocorrelated.

Table S1: Study area characteristics and imagery availability. The availability of the 1949 and 1969 aerial images is indicated by a cross and the satellite acquisition dates are reported. For each study area its surface area, number of lavaka and resulting lavaka density are indicated.

Study area	**Surface [km²]**	**Aerial picture 1949**	**Aerial picture 1969**	**Satellite aquisition date**	**Satellite source**	**Number of lavaka**	**Lavaka density [lavaka km^{-2}]**
1	11.47	X	X	27/05/2018	WorldView-2	153	13
2	10.47	X	X	12/09/2011	WorldView-2	128	12
3	15.29	X	X	10/07/2016	WorldView-2	140	9
4	10.48	X		29/05/2018	WorldView-2	173	17
5	11.27	X	X	27/05/2018	WorldView-2	55	5
6	11.98		X	27/05/2018	WorldView-2	50	4

Text S2 Figures

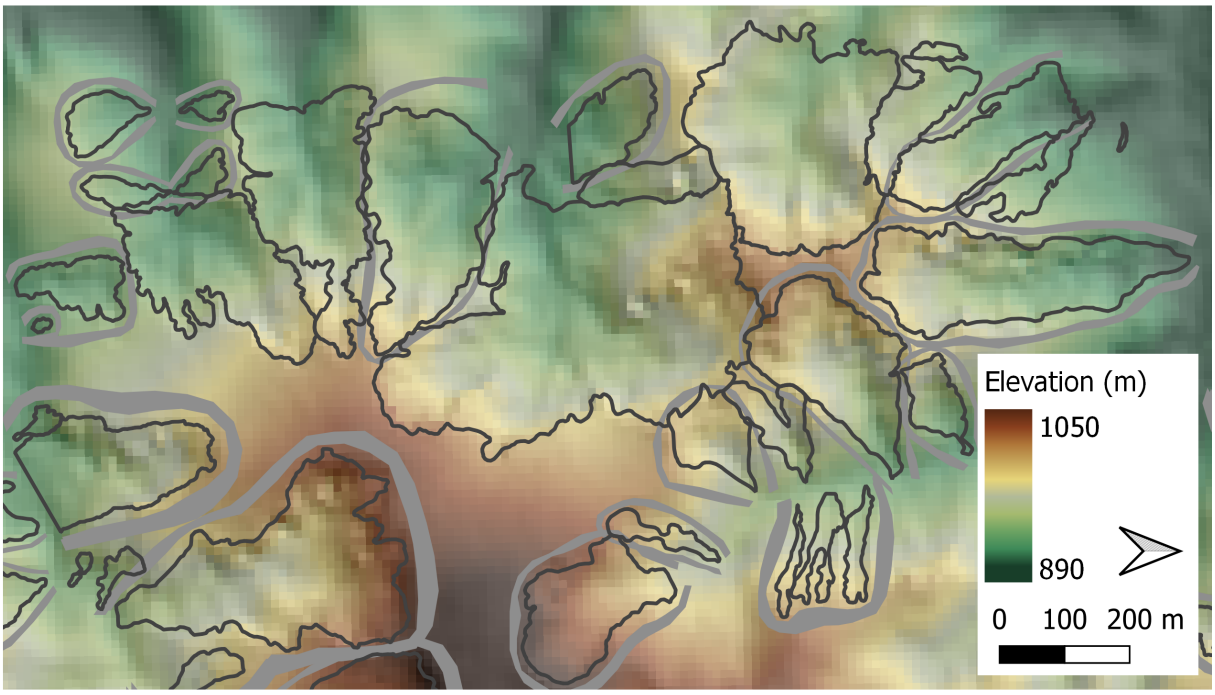

Figure S1: Example of near absence original surface topography. Example from study area 1 illustrating the near absence of the original surface topography (especially in the western part of the area) due to the dense presence of lavaka (dark grey outlines). Grey horseshoe-shaped polygons indicate the areas unaffected by gully erosion. These could not be derived for all lavaka, and sometimes envelope multiple lavaka that are located next to each other. Displayed elevations are from the TanDEM-X DEM with hillshade (Krieger et al., 2007).

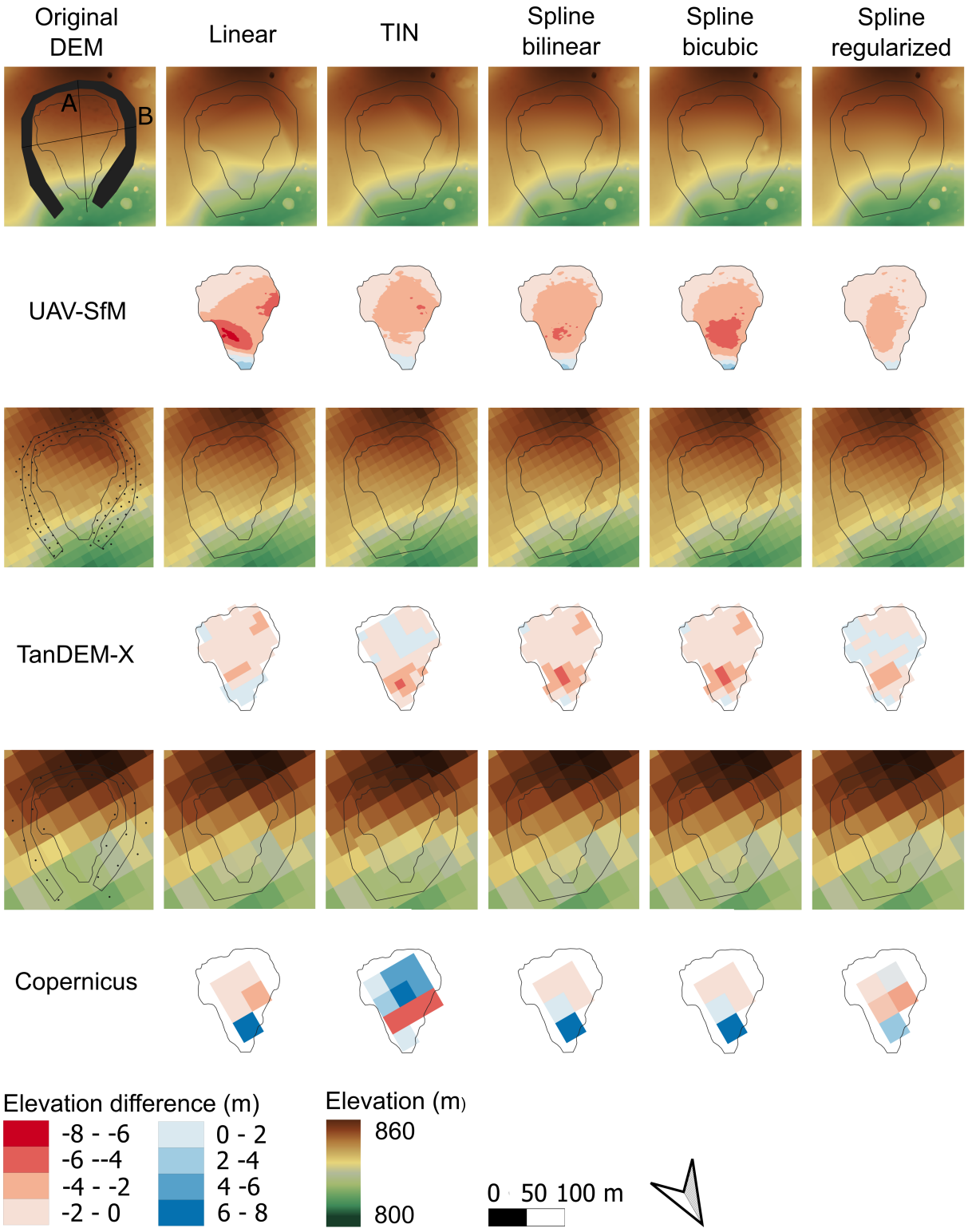

Figure S2: Interpolation error workflow. The interpolation error was assessed by placing 50 lavaka polygons and corresponding horseshoe-shaped polygons on intact hillslopes. The difference between the interpolated surface and the DEM gives the interpolation error. This is done for all three DEMs (UAV-SfM (0.2 m), TanDEM-X (12 m) and Copernicus (30 m)) and by using five different interpolation methods (Linear, TIN, Spline bilinear, Spline bicubic and Spline regularized).

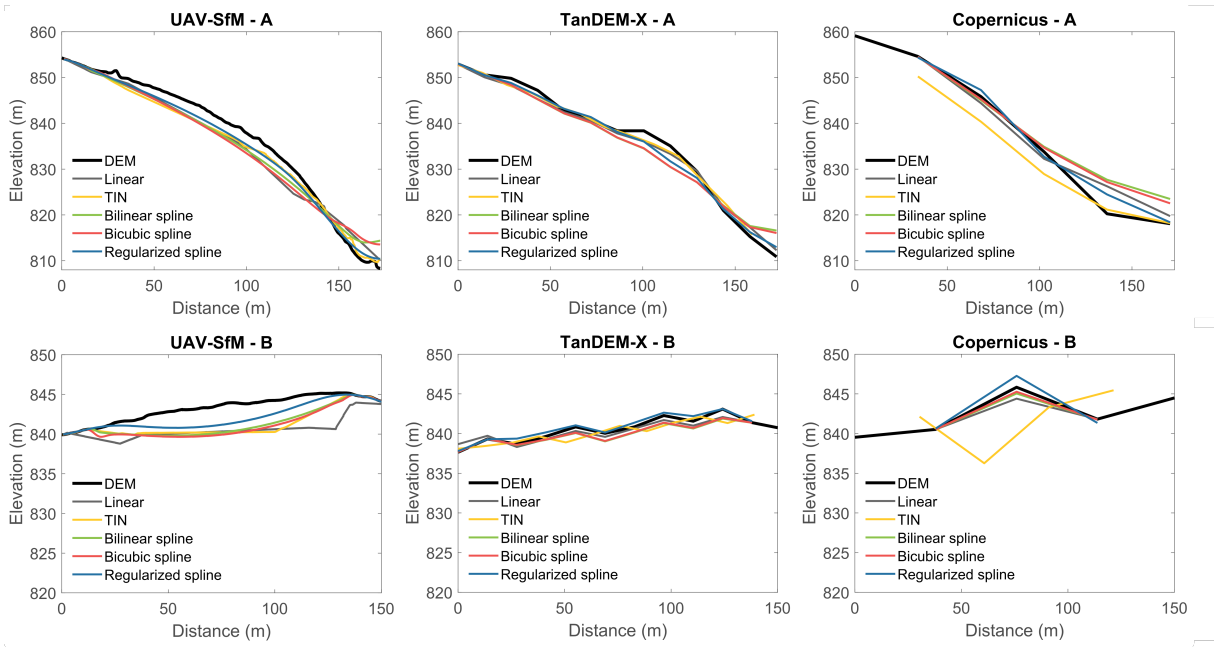

Figure S3: Interpolation error cross sections. Cross sections for transect A and B as indicated in Fig. S2 for each of the three DEMs (UAV-SfM (0.2 m), TanDEM-X (12 m) and Copernicus (30 m)) and five interpolation methods (Linear, TIN, Spline bilinear, Spline bicubic and Spline regularized).

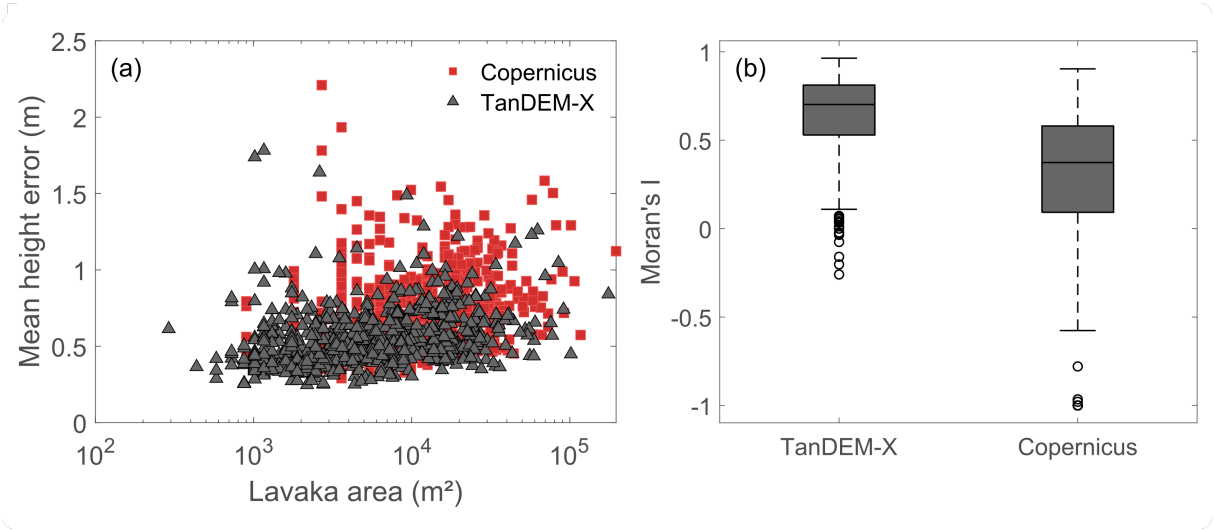

Figure S4: Relative height error. (a) The relative height error is estimated based on the Height Error Mask (HEM) of the TanDEM-X and Copernicus DEMs, which represent the random elevation error in the form of the standard deviation. A positive correlation between the mean height error of a lavaka and its surface area is observed. (b) The autocorrelation of the HEM-values is calculated for each lavaka by means of the Moran I (queen) for both the TanDEM-X and Copernicus DEM. A value of 1 represents a perfect positive autocorrelation, a value of zero a random distribution and a value of -1 indicates negative autocorrelation.

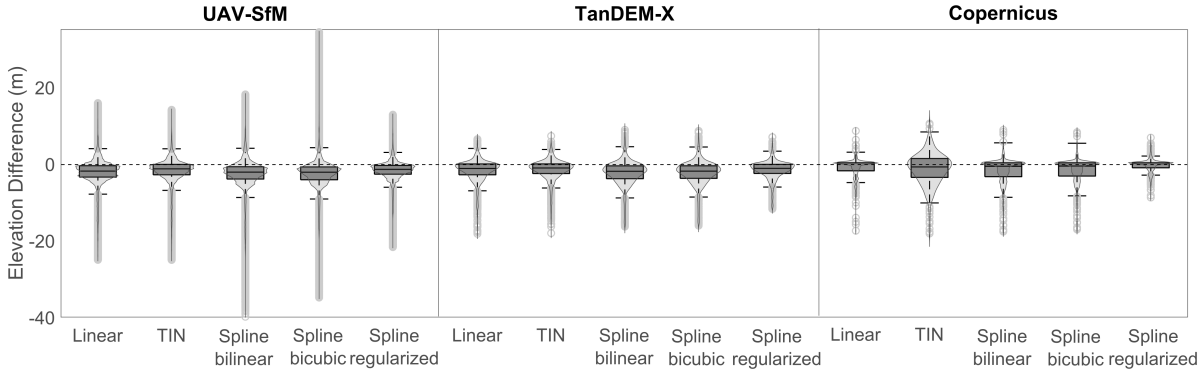

Figure S5: Interpolation error. The calculated elevation differences between the interpolated surface and DEM surface respresent the interpolation error and are displayed as violin plots overlaid by boxplots. The interpolation error has been determined for all three DEMs (UAV-SfM (0.2 m), TanDEM-X (12 m) and Copernicus (30 m)) and for five interpolation methods (Linear, TIN, Spline bilinear, Spline bicubic and Spline regularized). The distribution of the full dataset containing all the individual pixels is displayed.

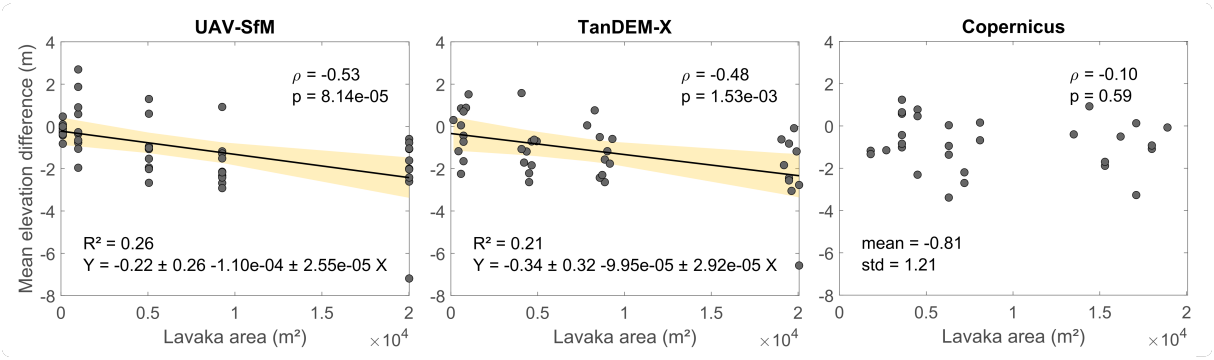

Figure S6: Mean interpolation error vs. lavaka area. The correlation of the mean interpolation error, i.e. the difference between the interpolated and DEM surface, per lavaka is verified for all three DEMs: UAV-SfM (0.2 m), TanDEM-X (12 m) and Copernicus (30 m). For the Copernicus DEM a significant correlation between both factors is absent $\rho = -0.10$, p = 0.59. The mean elevation difference of -0.81 ± 1.21 m is used for all lavaka in the case of Copernicus. For the UAV-SfM and TanDEM-X DEM a significant decrease in mean elevation difference is observed with increasing lavaka area ($\rho = -0.53$ and -0.48, respectively with $p < 0.05$). The linear relationship between both factors and corresponding uncertainties are used to assess the interpolation errors in these cases. The shaded area indicates the 95% confidence intervals of the fitted relationships, reported uncertainties on the a and b coefficients are the standard deviations.

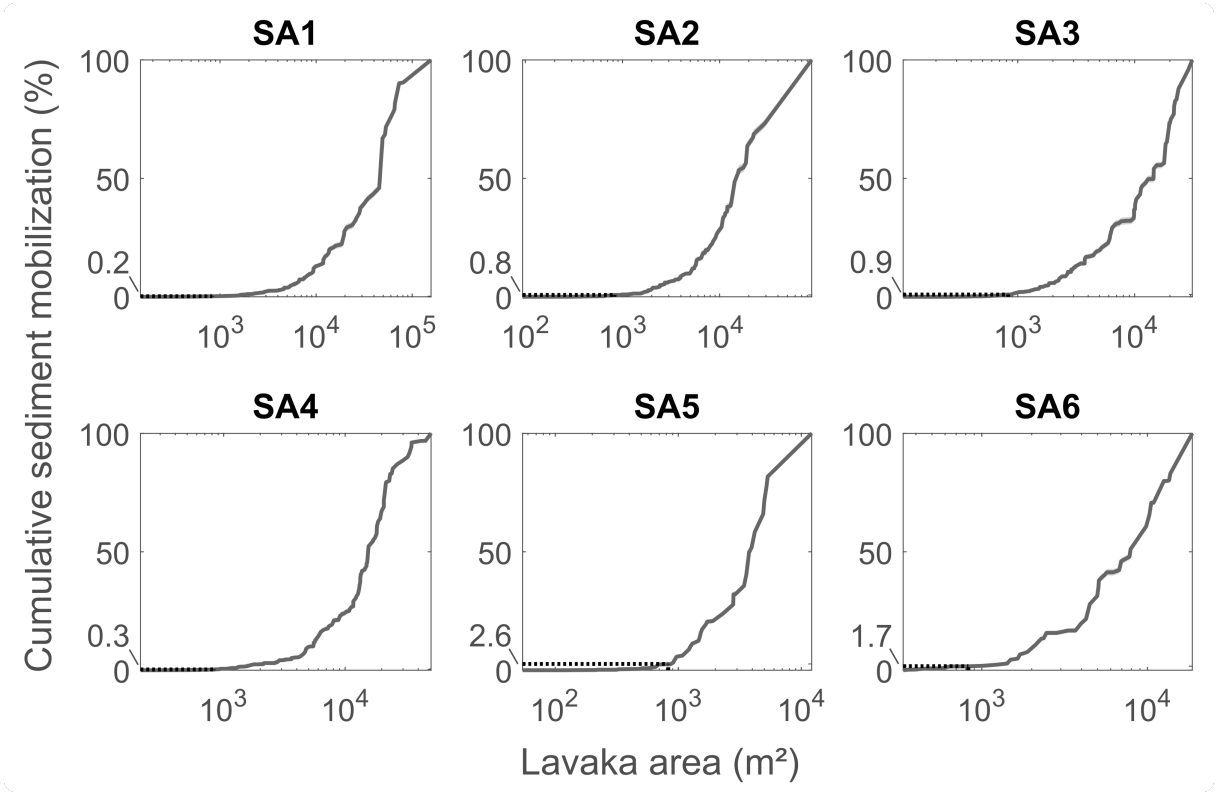

Figure S7: Cumulative lavaka sediment mobilization per study area The relative cumulative lavaka sediment mobilization is plotted as a function of lavaka area for all study areas. The fraction of sediment supplied by lavaka smaller than the identified TanDEM-X threshold (800 ± 250 m^2) is indicated by the black dotted lines. This fraction is also added to the y-axis. Note that the lavaka areas are plotted on a log-scale.

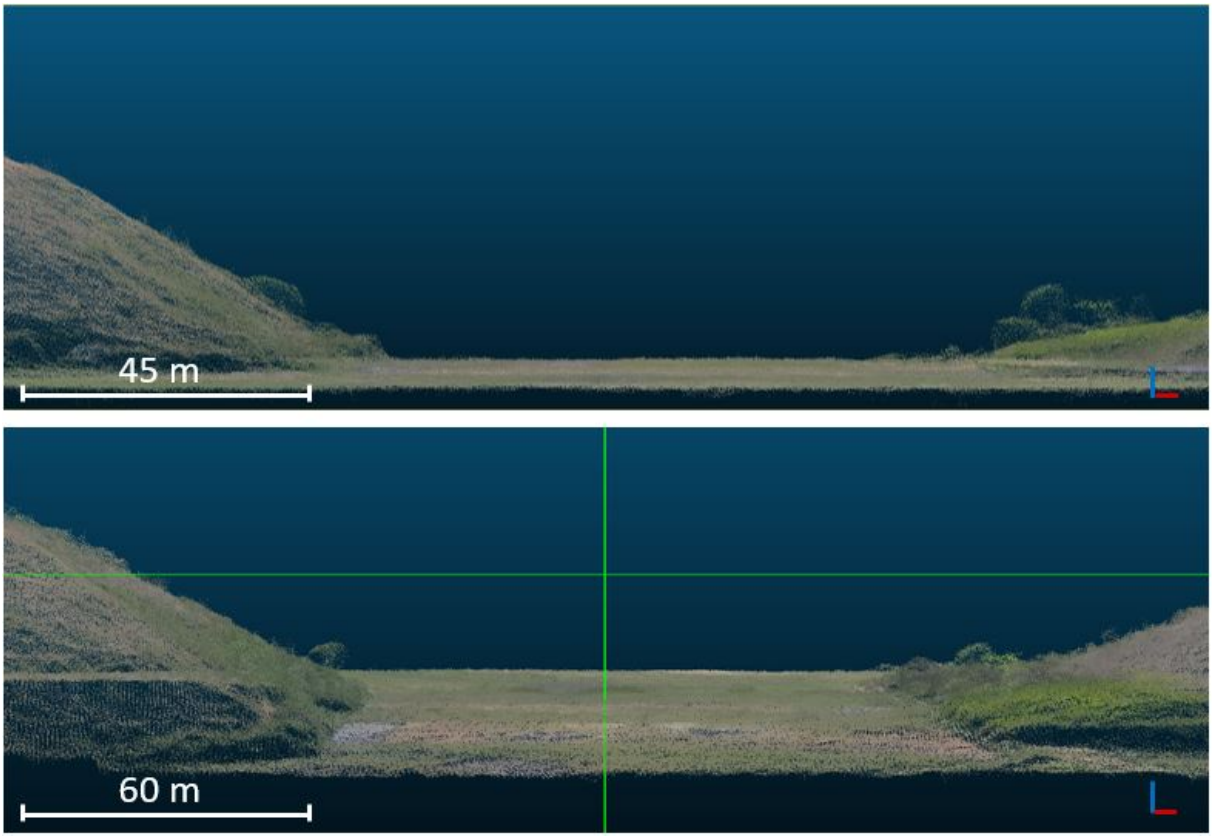

Figure S8: UAV-SfM point clouds over flat areas. In order to verify the presence of vertical doming due to the use of a fish-eye lens for the UAV-SfM DEM, the point clouds are visually inspected over flat surfaces. Visual inspection does not indicate the presence of vertical doming.

References

Krieger, G., Moreira, A., Fiedler, H., Hajnsek, I., Werner, M., Younis, M., and Zink, M.: TanDEM-X: A Satellite Formation for High-Resolution SAR Interferometry, IEEE Transactions on Geoscience and Remote Sensing, 45, 3317–3341, https://doi.org/10.1109/TGRS.2007.900693, 2007.